# Chapter 7

# Functionality Assessment of Scaffold under Biomechanical Loading

## 7.1 Introduction

Previous research has shown that the application of traditional solid implants resulted in a mechanical mismatch with the surrounding bone [8–12]. Primarily the effective modulus mismatch results in the stress shielding effect which often becomes primary reasons for implant failure in postoperative period. In chapter-5, it was demonstrated how Young's modulus decreases by introducing the pore in the solid volume. In this chapter, this validated concept is interpolated to generate an anatomically matched scaffold mimicking large bone defect on the femur bone and demonstrated how stress shielding effect is reduced. To this aim, this chapter is determined on the development of 3D model of femur bone and generation of anatomically matched scaffold. Finally, the stress transfer mechanism at bone-scaffold interface is presented.

In most of the studies, the patient specific reconstruction is reduced to either pilot studies or by idealization of arbitrarily generated CAD model or most of the studies have been simplified to two-dimensional analysis [Rudman et. al. 2006, Ueo et. al. 1987]. There are several reasons which may either be the time-consuming process of the development of these model or difficulty in obtaining research specific patient data or may be due to complexity of introducing complex geometrical variables.

The importance of patient specific implant can be explained by several classic examples. In context to the large segmental bone defect here, the importance is provided in chapter 1. More specifically, an example of complex spine model will be more classic demonstration to understand the importance of specific development. We all know that the spinal owes a complex representation from its spinous process to its facets rather than a perfect prismatic and cylindrical representation (Dreischarf et al. 2014, Chan et al. 2021), to accurately estimate the range of motion of the computational model it is essential to include patient-specific contour data when studying the degradation behaviour of intervertebral disc, but few years back most

of the numerical reports on the biomechanical results were on the approximated model and most of the researchers deemed a validated results and cited to their research .

Recently, CAD models of specific human structures for the numerical analysis or additive manufacturing have recently gained attention due to the advancement of image-based algorithms implementation for calculation of 3D models in various commercial softwares. These software usually employ medical images of X-Rays, CT/MRI or ultrasound images to develop 3D model, which are now become a template for computational 3D model generation (Arbabi et al. 2007, Gilles et al. 2006) to establish the patient-specific models.

Since, dealing with extraction of small models sufficiently requires less effort, while identifying region of interest (ROI) for large models such as long femur bones, working and segmenting ROI on each image is tedious and time-consuming task. Many softwares offers semi-automated algorithms to extract ROI from each image data. However, to make the balance between the quality and quantity of the obtained model it usually requires to work manually on particular image sets (Figure 7.1).

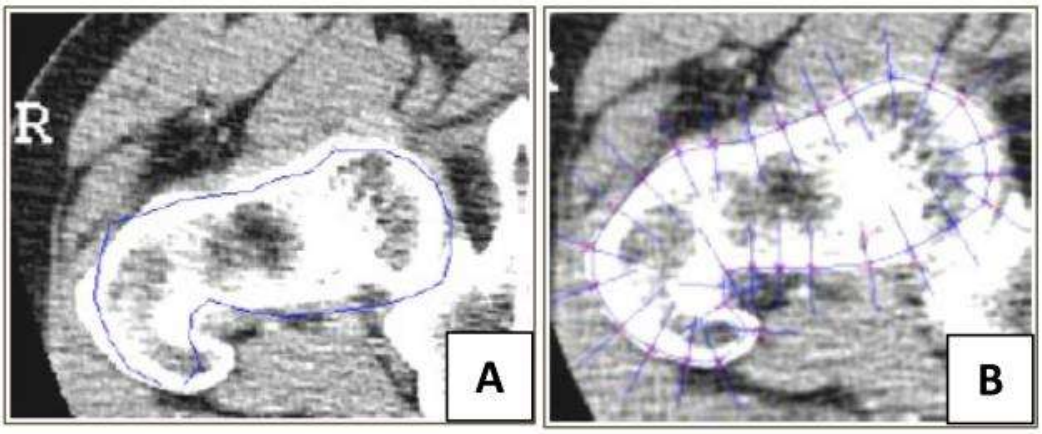


**Figure 7.1:** (A) Boundary contour to detect bone region on the medical image (B) Search lines from each control points to control fit of contours converge to or diverge from the centre to predict the contour on the subsequent slices (Safont et al. 1999).

Many improvements in 3D model generation have since been made and implemented in the commercial software like 3D-Doctor, Simpleware scan IP, 3D slicer, Rhinoceros etc. In this work, the creation of the 3D femur model was originally done through Mimics 18.0 (Materialise, Leuven, Belgium) by processing CT medical images. The main stages of model creation are: collection of CT scan data (image acquisition), generation of anatomical structures from CT scans (image segmentation, 3D model reconstruction and optimization), development of solid model of femur and surgical simulation of critical size bone defect. CT data of a patient's lower extremity is used to develop 3D model of femur bone. The steps involved in this process are discussed in detail.

The development of 3D femur model used in this research work was performed through Mimics 18.0 (Materialise, Leuven, Belgium) by processing CT medical images. The steps to develop 3D model of femur include: collection of CT scan data (image acquisition), generation of anatomical structures from CT scans (image segmentation, 3D model reconstruction and optimization), development of solid model of femur and surgical simulation of critical size bone defect. CT data of a patient's lower extremity is used to develop 3D model of femur bone. The steps involved in this process are shown below in Figure 7.2 and discussed in detail in this section.

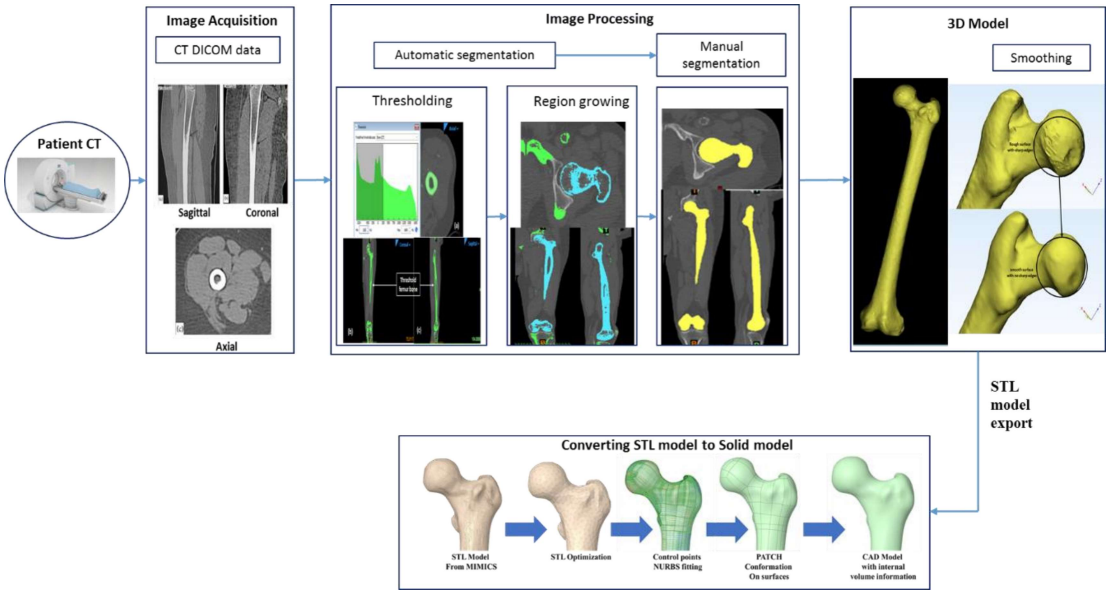


**Figure 7.2:** Illustration of the steps involved in the process of development of 3D model of femur and conversion of STL model to solid model.

Images in the XY plane (axial images) are typically stacked and imported into the MIMICS software. After that, the software computes and generates pictures in the XZ (coronal) and YZ (sagittal) directions. This allows for a more detailed 3D representation of the 2D data.

### 7.2 Image acquisition

Each medical imaging modality has a specific physical principle so as to provide characteristic in vivo image data for various tissue types within a body section. For the geometric modeling of patient-specific anatomy, it is essential to select a proper imaging modality. Whenever opting for the imaging modality, some of the features like contrast-to-noise ratio, signal-to-noise ratio and image artefact types must be considered seriously. CT images are best suited for bone modeling in case of orthopedic applications, as high contrast is used for hard tissues as compared to soft tissues. On the contrary, MRI images are more suitable for modeling of soft tissue due to the greater tissue resolution, where it is easy to distinguish tendons from muscles and cartilage from bone. Although CT scans are more costly and take longer to

complete than MRI scans (which also demand greater energy outputs), CT scans have higher radiation requirements for higher resolution.

To generate a model of a specific anatomical structure it is necessary, first of all, to identify the tissues that compose the organ(s). Then, according to the desired image features, an appropriate medical imaging modality is chosen for data acquisition. For all cases here reported CT imaging is the proper selection.

Therefore, 3D FE model of the healthy human femur was reconstructed by CT-DICOM images using image processing algorithms that included the main structures of lower extremity. A standard CT scan procedure is followed to obtain cross-sectional images of femur anatomical locations from the subject to generate a femur solid model. A written and informed consent followed by guidelines approved by the Ethical Committee of the Institute of Medical Sciences, Banaras Hindu University, is obtained on the use of computed tomography (CT) images. Copy of ethical permission is attached at last.

CT images represent a map of pixel containing the tissues with a linear X-ray attenuation coefficient (Nareliya et al., 2011). Each pixel value is scaled in a manner such that the linear X-ray attenuation coefficient of air is equal to -1000 and that of water is equal to 0. This scale refers to the Hounsfield scale (HU) or CT numbers (Figure 7.3) named after one of the pioneers in CT, Godfrey Hounsfield. It is a quantitative scale for describing radio density, can be calculated as:

$$HU = 1000(\mu_x - \mu_{water})/\mu_{water}$$

Where, $\mu_x$ = Average linear attenuation coefficient in a voxel, $\mu_{water}$ = Linear X-Ray attenuation coefficient of water.

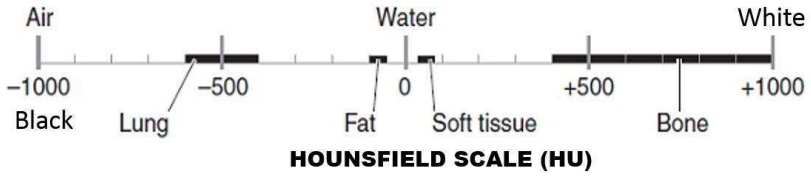


| Substance | HU |
|---|---|
| Air | −1000 |
| Lung | −700 |
| Soft Tissue | −300 to -100 |
| Fat | −84 |
| Water | 0 |
| CSF | 15 |
| Blood | +30 to +45 |
| Muscle | +40 |
| Bone | +700(cancellous bone)to +3000 (dense bone) |

**Figure 7.3:** Hounsfield scale showing a range of Hounsfield Unit for body system.

The DICOM patient-based coordinate system is right-handed. The X-axis is towards the patient's left side, the Y-axis towards the patient's posterior, and the Z-axis to the patient's head. (Figure 7.4).

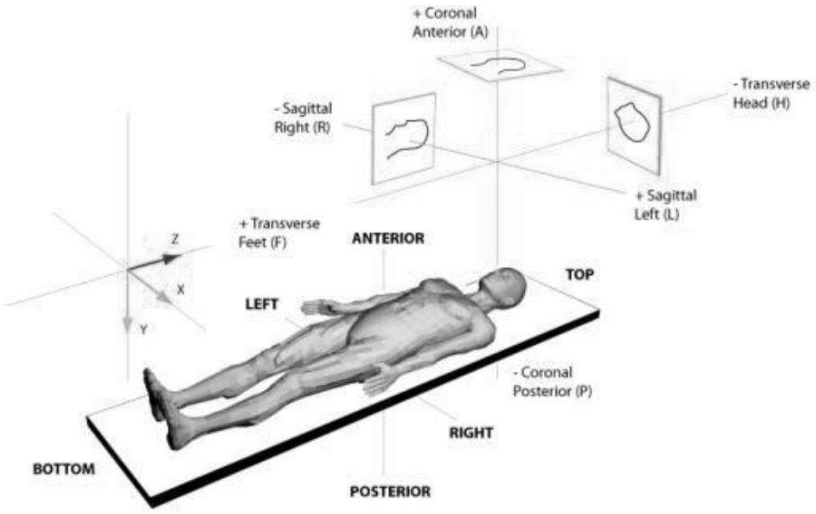


**Figure 7.4:** DICOM patient-based coordinate system.

A 64 slice CT scanner from GE Medical System was utilised to obtain CT scans by aligning the patient's lower extremities to the CT scanner and moving it clockwise. Apparatus power

condition were at 120 KV/350mA. The images obtained were in DICOM format (Digital Imaging and Communication in Medicine) and imported directly to Mimics software.

The development of 3D femur model used in this study was originally done in Mimics 18.0 (Materialise, Leuven, Belgium) by processing CT medical images. Mimics makes use of 2D cross-sectional medical images from imaging modalities like computed tomography (CT) to build 3D model that may be directly interlinked with CAD software for surgical simulation and FE analysis. An acquired set of images can be directly imported in the Mimics software which usually contains images in XY plane (axial images). Furthermore, it calculates and generates images in the XZ (coronal) and YZ (sagittal) directions, allowing for a more exact 3D representation of the 2D data.

To develop a three-dimensional (3D) reconstruction of the femur bone, Materialise MIMICS 18.0 (Materialise, Leuven, Belgium) software is utilised. The images have a resolution of 512x512 with the slice thickness of 0.625 and 0.833984-pixel spacing. The slice spacing and quality of pixel guarantee the coherent dimensional reproducibility of the 3D models (Figure 7.5). The slice thickness also has an impact on the quality of the 3D model; a slice that is excessively thick can lose substantial information between neighbouring slices, resulting in poor contour identification.

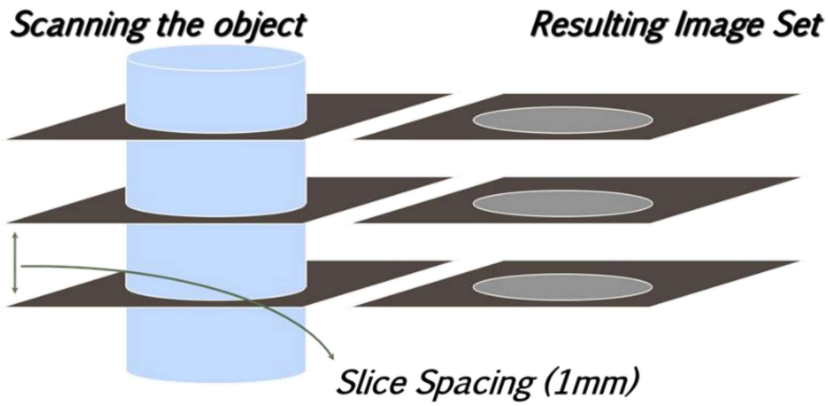


**Figure 7.5:** Schematic illustrating the process of data acquisition.

### 7.2.1 Preparing the acquired CT Data

The Mimics software enables for the automated import of the CT scans with a total of 529 slices. The data were imported and converted at this stage by selecting "Import Images" from the "File" menu, then altered orientation. The orientation settings are required for MIMICS to display images accurately. In presence of signal noise and image artefacts it is essential to improve the resolution and quality of the CT images by appropriate acquisition parameters tuning as slice thickness and spatial resolution. Also, several digital image processing techniques can be applied in order to enhance the visual information contained in an image.

#### 7.2.1.1 Windowing

The grey values of CT scans are represented using the Hounsfield scale that has 4096 values. Mimics features a function called windowing that allows you to transfer this scale onto your computer's 256 grey values. Windowing is a technique for adjusting visual contrast (Figure 7.6).


**Figure 7.6:** Clear distinction between a preset bone scale and a soft tissue scale is used to set the contrasts in Mimics 18.0 (Materialise, Leuven, Belgium)

Differences between soft tissues, fat, muscles as well as bones can be visualized on the basis of the window selected. For best resolution, the contrast tool contains a grayscale which has

certain predefined scales. Each set of scale has a fixed minimum and maximum value, enlisted in Table 7.1.

**Table 7.1:** A range of predefined Grayscale with maximum and minimum values.

| Grayscale | Minimum value | Maximum value |
|---|---|---|
| Custom Scale | -1024 | 350 |
| Bone Scale | -1024 | 1590 |
| Soft tissue Scale | -150 | 350 |
| Narrow Scale | -900 | 1100 |
| Wide Scale | -1024 | 1590 |
| MRI Scale | -1024 | -524 |

#### 7.2.1.2 Volume Rendering

Volume rendering allows for the immediate visualisation of 2D images as a 3D model without the need to segment and develop a model. It is merely a visualisation tool that provides a good idea of how the model will appear (Figure 7.7). Volume rendering uses a significant amount of system memory, which slows computational time, thus it's disabled after visualizing.

**Figure 7.7:** Image showing bone scale volume rendered data.

### 7.2.2 Extraction of material properties from CT data

Prior research suggests that the link between Hounsfield Units and mechanical parameters, which may be obtained from greyscale data, is strong enough to allow usage in FE (Les et al., 2005). To find a connection between apparent density and Hounsfield Units for the CT-data, a phantom should ideally be scanned simultaneously with the subject (Taddei et al., 2007). Based on the experimentally obtained correlations, material stiffness may then be connected to apparent density. In order to determine the boundaries of cortical and trabecular bone when a phantom is not available, the connection between apparent density and Hounsfield Units are sometimes approximated by looking at the CT-data (Majumder et al., 2007). The CT-scans employed in this investigation had no phantoms. While certain density stiffness correlations also consider the cortical area, the majority of them simply consider trabecular bone. Helgason et al. found significant inter-study variances in their comparative analysis of all predictive correlations, however this was based on research that focused on various bones in the body, so discrepancies are to be assumed (Helgason et al., 2008).

## 7.3 Segmentation and 3D reconstruction of femur bone

Segmentation is the key to transforming anatomical data from images to 3D models. The imported data is in the form of slices that can be visualised in three different planes namely, the sagittal, frontal, and axial views. In the sliced picture data, segmentation highlights the structure(s) or region(s) of interest. Grayscale information is present in medical pictures produced by CT or MRI scanners. Mimics enables to generate models based on the grey value (Hounsfield units in CT scans) included in these images. The colour (white, grey, or black) of a pixel in images is indicated by a number known as the grey value. The material density of the scanned entity is directly related to the grey values corresponding to each pixel in the image data. As a result, Mimics may construct models from any shape recognisable

within the scanned dataset. Automatic segmentation including threshold and region grow method, followed by manual segmentation and smoothing is performed to generate the 3D model of femur bone.

### 7.3.1 Automatic segmentation

This process as the name suggests is an automatic process which is applied on all the slices of data at once irrespective of the specific region of interest. It includes two main processes mention below.

#### 7.3.1.1 Threshold

Image data may be segmented and models developed by combining up comparable grey values. This method of segmentation is known as thresholding, and it produces accurate models. It is necessary to fix the threshold value precisely since different anatomies will have differing grey values in CT images. When the threshold value is established, we may examine the CT images to see the needed portion of the retrieved organisations. To avoid noise, the threshold should be set as low as feasible. A decent Mimics threshold value is around 270 (Hounsfield scale). Figure 7.8 depicts the thresholding procedure.

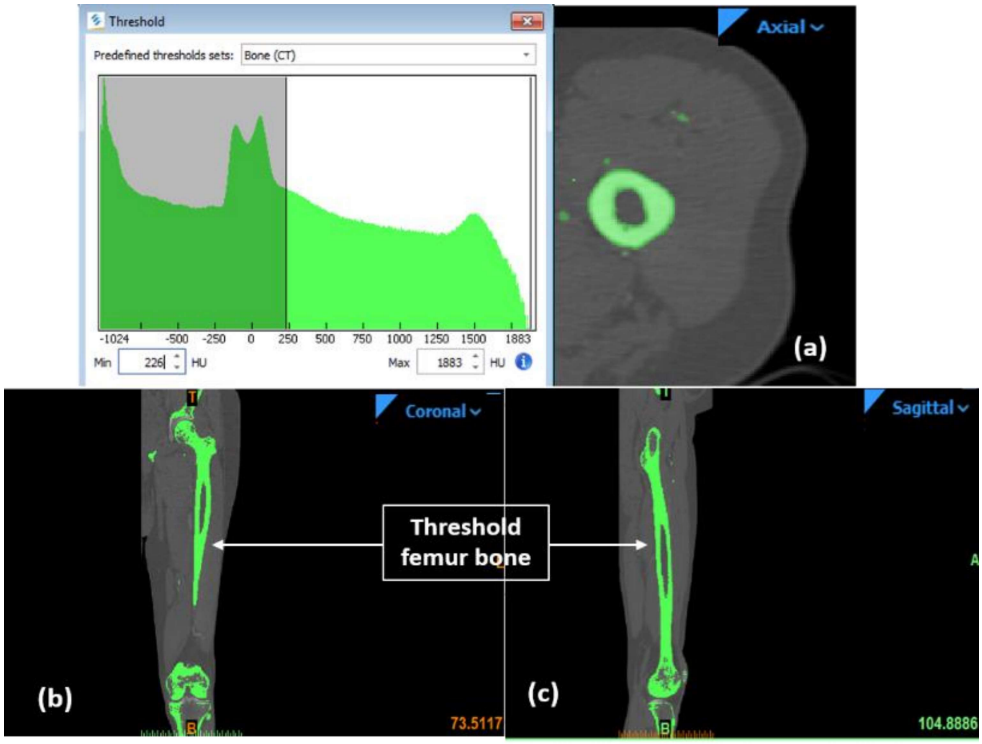


**Figure 7.8:** CT images of femur bone are thresholded with Bone (CT) scale. (a) Axial (b) Coronal (c) Sagittal View.

The same colour or mask is used to classify all pixels within a Hounsfield range. For various biological components specified in the threshold toolbar, preset scales are available. A lower threshold is used to separate soft tissues, while a higher threshold is utilised bone segmentation. The threshold values are used to see how various thresholds highlight different regions of the image. In this procedure, the preconfigured bone (CT) setting of 226 to 1883 is a good bone threshold (Figure 7.9). Therefore, for selecting bone on CT images, the lower threshold is set on 1/3 of the cortical peak.

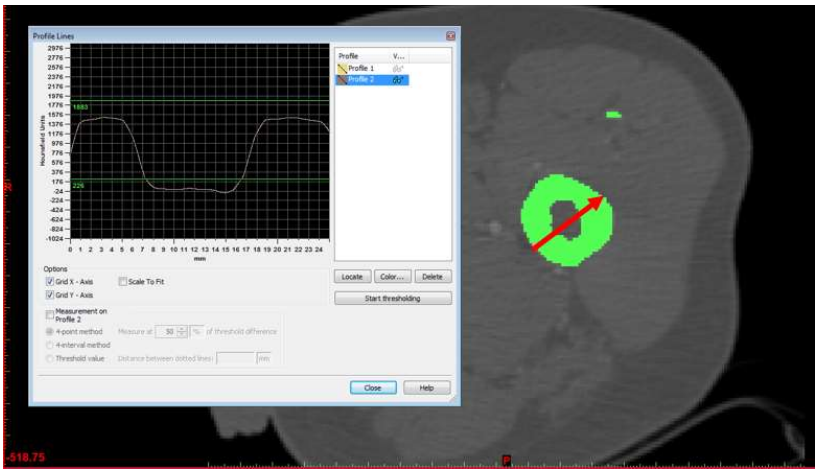

**Figure 7.9:** Profile line graph illustrating the threshold range for bone (CT).

### 7.3.1.2 Region Growing

It is an automatic partial segmentation process which separates the masks in different fragments and helps to remove the floating pixels so as to obtain the desired region (Figure 7.10).

The purpose of applying region growing segmentation was that, though, complete segmentation is not provided in a single step, however it enhances the parts near the complex regions with a new mask so that the complete region of interest can be visualized properly (Figure 7.11). This makes the next step of manual segmentation much easier.

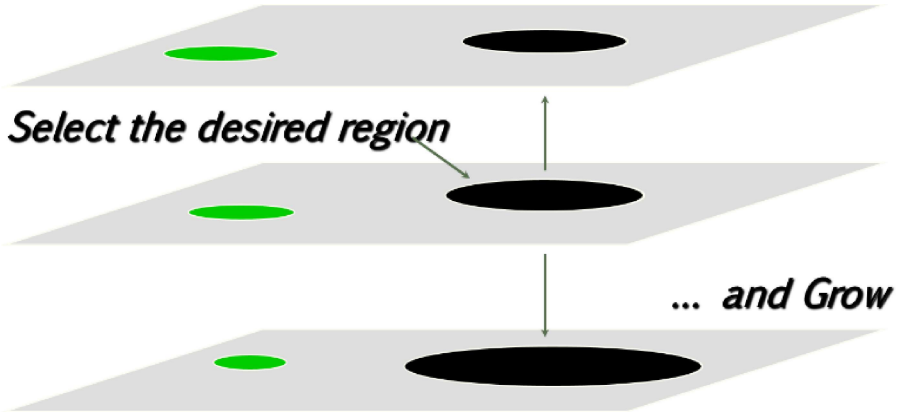


**Figure 7.10:** Illustration of the region grow process.

### 7.3.2 Manual segmentation (Edit mask)

The active mask is used for all manual editing operations. In order to preserve the original geometry, it was essential to keenly observe the pixels and segment them accordingly. Manual segmentation is performed by using edit mask tool which helps to erase, draw or even re-establish the image with a certain value of threshold. This method is performed after region growing in order to achieve complete segmentation of region of interest, resulting in a more continuous surface (Figure 7.11). Therefore, exact geometry can be extracted from the CT scan images so as to obtain a perfect 3D geometry.

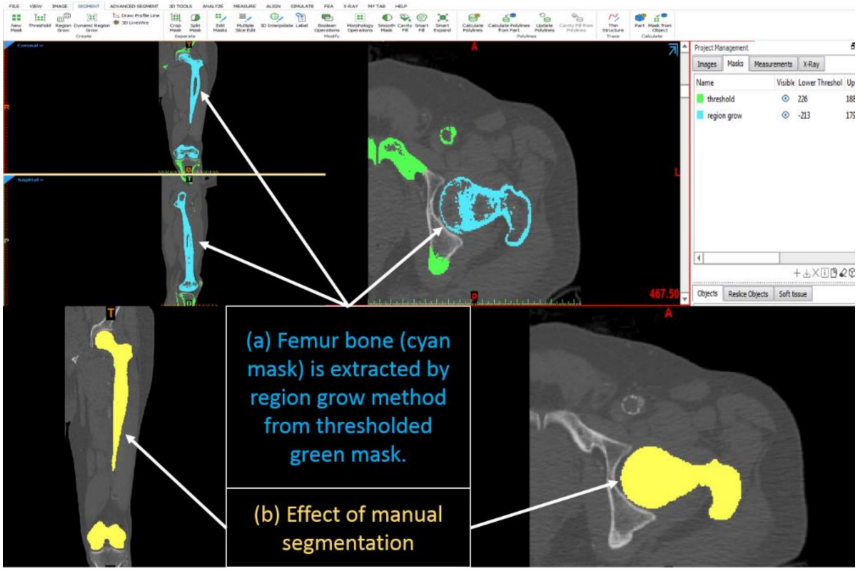


**Figure 7.11:** Effects of region grow followed by manual segmentation to develop accurate 3D model.

After carefully completing all the above mentioned steps custom parameters are set in "Calculate 3D" tool to calculate three dimensional model using "Segmentation" menu to generate 3D model of femur bone (Figure 7.12). The 3D model of the femur can be visualized in the 3D view. The 3D reconstruction relies on 3D interpolation methods to convert 2D images (slices) into a 3D model. Gray levels interpolation was utilised in conjunction with the accuracy

method for this reconstruction procedure to achieve more consistent volumetric representations of the femur bone.

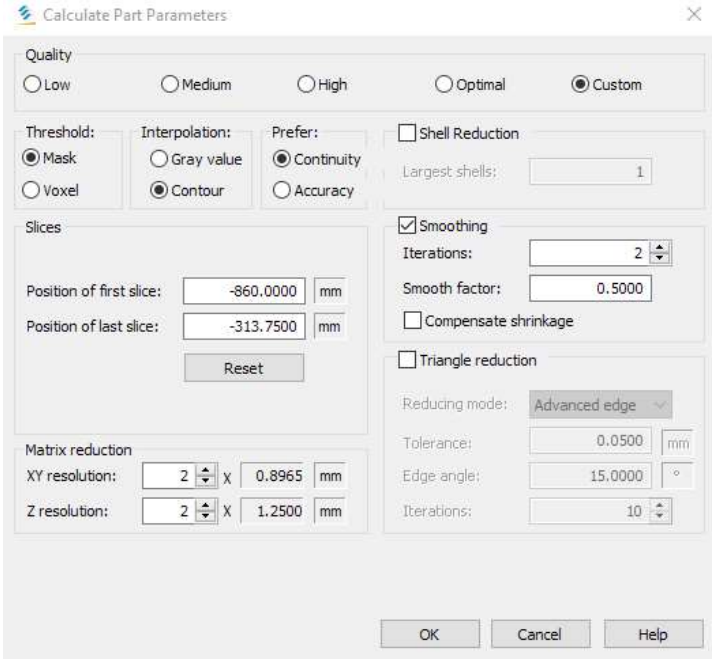


**Figure 7.12:** Illustration of 3D reconstruction process of femur bone in MIMICS software.

### 7.4 Calculate 3D

Mimics can construct a 3D model using the segmentation, together with known details like the pixel size and also the spacing between image slices. The precision of a Mimics model corresponds to the accuracy of an entity acquired by scanning. Here the created masks with the lower and higher threshold mentioned above are listed. We selected the desired mask from which 3D model was to be created (Figure 7.13).

**Figure 7.13:** 2D CT images converted to 3D model using Mimics Software.

An optimal quality was selected to convert the region grown mask into a 3D model. Finally, 3D model was calculated with a red mask for complete femur bone geometry as shown in Figure 7.14.

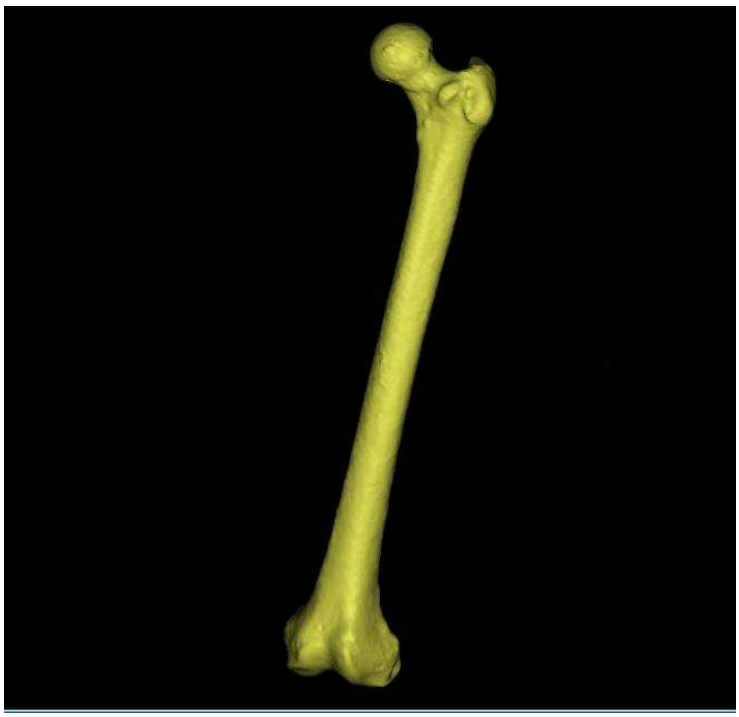

**Figure 7.14:** Developed 3D model of femur bone structure.

## 7.5 Smoothing

Since, the model generated by the above process is not accurate and has a rough surface with spikes (Figure 7.15 a), smoothing operation is applied to generate a smooth model (Figure 7.15 b). Iterations are carried out by setting a smooth factor between 0 and 1. Finally, the accurate 3D model is generated.

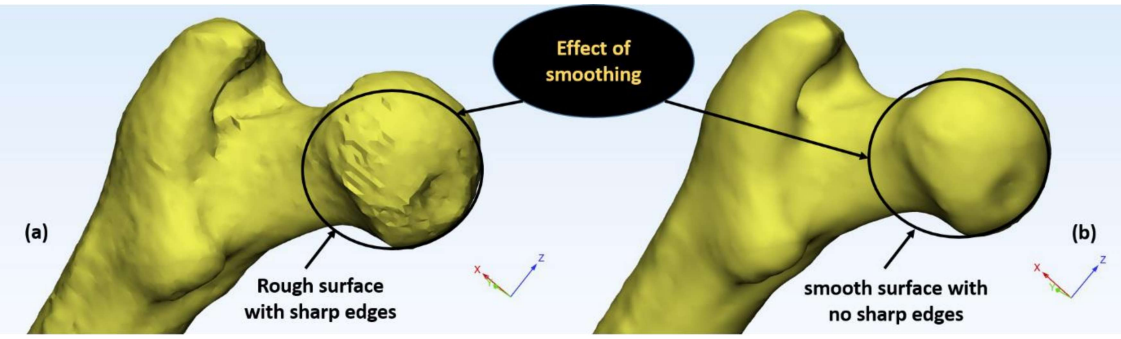


**Figure 7.15:** Effect of smoothing on developed 3D model. (a) Rough surface with sharp edges, (b) Smooth surface with no sharp edges.

## 7.6 Optimization

Since, the developed 3D model shows errors in the form of holes, overlapping triangles, inverted normal, bad edges, holes, etc., that may affect its performance when used in further FE simulations. Hence, these errors essentially need to be minimized as much as possible. This can be done using 'Fix' tool. The 'Fix Wizard' tool in 'Fix' menu and toolbar is used to run the quality check of the developed 3D models. It has a diagnostic function, i.e. a diagnostics page, which is the key-step in the Fixing Wizard that determines any errors associated with the STL-file. Automatic fixing followed by manual fixing of errors is performed. The steps followed are similar to those as explained in Chapter 3.

Further, remeshing is done using 'uniform remesh' tool to remesh the model while preserving its geometry. This tool offers finer control over the generated mesh, and can even restrict the

remeshing to a small region of interest; however, depending on the parameters, there is a possibility of minor data loss that can be minimized to some extent using 'preserve sharp edges tool'. The model is checked again for any errors and if found any, are fixed again as mentioned above. These steps are repeatedly followed until no further reduction is possible. Finally, an optimized model is obtained that are exported in .STL format to be used for surgical simulation of scaffold.

### 7.7 Surgical simulation of patient specific scaffold

The developed femur model is than imported in ANSYS SPACECLAIM software to create the intentional segmental bone defect to assess the mechanical performances on the use of porous scaffold. However, details about size and causes of the segmental bone defect and bone defect in large bones were already discussed in Chapter 2 in detail. Here we directly present the creation of critical size defect with specifically matched patient anatomy. The purpose of creating intentionally generated bone defect on femur to demonstrate the stress transfer patterns from bone to implant to actualize the reduction of stress shielding.

### 7.8 Boolean intersection of porous structure on the solids

On the basis of a hybrid distance field and TPMS approach, Yoo et al. suggested an efficient method for the development of 3D porous scaffolds (Yoo et al. 2011). An virtually defect-free porous scaffold with a complex microstructure and high-quality external surface, appropriate to a particular anatomic model, can be simply generated without difficulties of trimming and re-meshing procedures by effectively incorporating a classic distance field method into the Boolean operation of the anatomical model and TPMS-based unit cell library. The Boolean operations between anatomical model and TPMS-based unit cells are depicted in Figure 7.16.

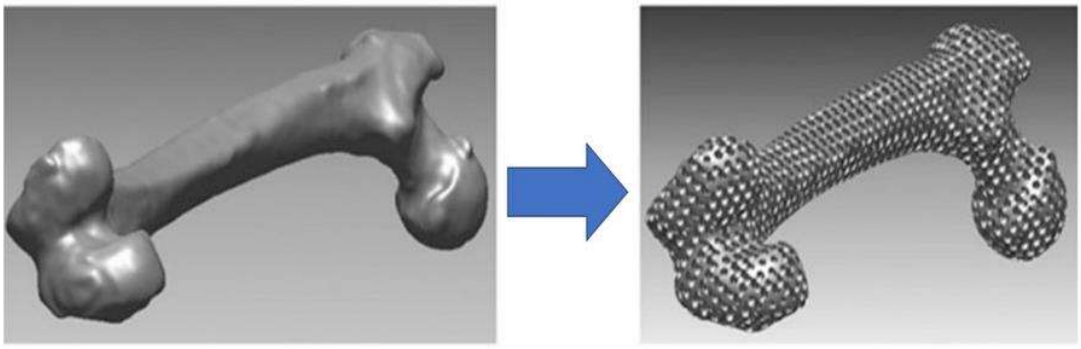


**Figure 7.16:** Porous scaffolds with complex internal structures and high-quality exterior interfaces (Yoo et al. 2011b).

It is possible to construct porous structures based on an array of repeating units by understanding the structure of the titanium alloy employed. The combine tool, which is a tool in the 3D design software SPACECLAIM, Because of a parametric design process, it is possible to design and produce the porous implant (Ran et al. 2018, Grunsven et al. 2011). It is feasible to produce a porous structure composed of a single closed entity from a Boolean intersection of bodies using this approach. (Zhang et al. 2018).

### 7.9 Designing exterior and interior geometry to achieve anatomical compatibility

The previously discussed method of reconstructing the femur bone from reverse-engineered CT data effectively converts STL model into solid model (Detailed procedure is mentioned in chapter 3 for TPMS structures conversion, same procedure is followed to convert the femur STL model into solid). By using porous TPMS unit cells, it is possible to create a scaffold with regulated exterior and internal architecture. The following hypothetical study demonstrates how a seeded implant might be constructed and utilised to repair a significant defect.

To develop the customized scaffold, first obtain CT data, segment the femur bone, then generate the STL model using the techniques outlined above. For obtaining 3D solid model, the .STL model of the femur generated from MIMICS was processed by following the steps as

discussed in Chapter 3. The solid model was exported in .STEP format. The complete step-by-step procedure is explained in Figure 7.17.

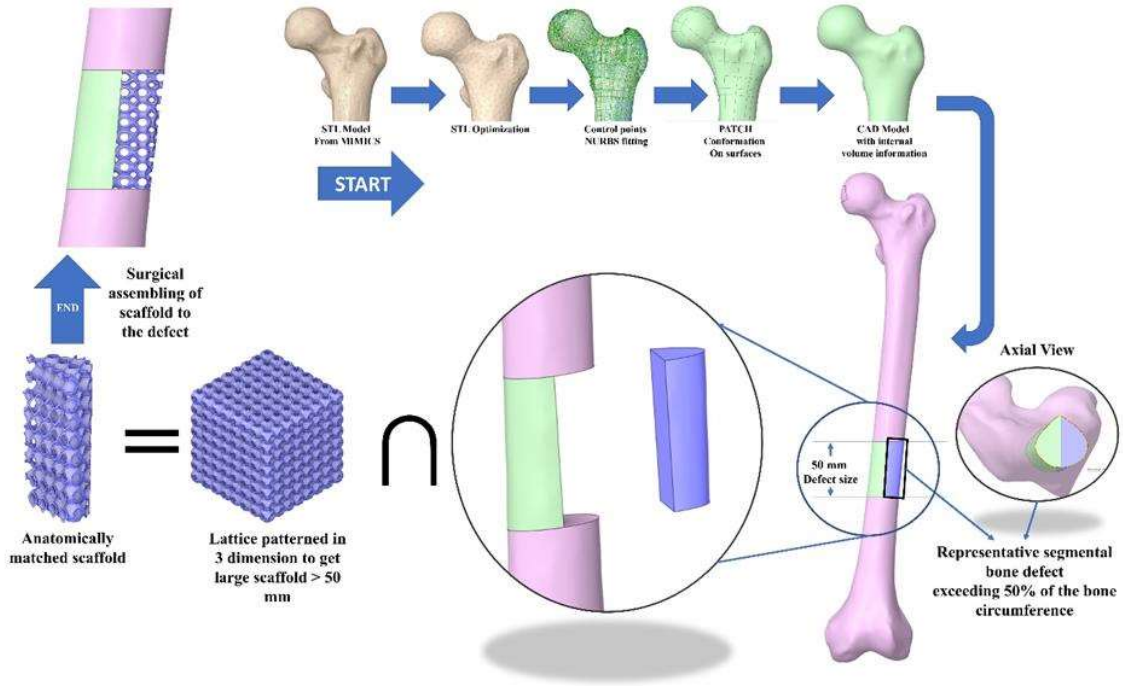


**Figure 7.17:** Schematic representation of complete process involved in the development of patient specific scaffold to treat segmental bone defect.

A section cut of 50 mm on the femur bone is performed to surgically create the segmental bone defect. However, it should be highlighted that the segments representing critical defects are chosen at random and do not reflect a real-world problem against which the implant attempts to intervene in clinical practice. The unit cell recruited for this study is P with 80% Porosity and is scaled from 1×1×1 mm to 6.28×6.28×6.28 mm on the same porosity of 80% to reduce significant computational cost (both time and memory) irrespective of utilizing the studied unit cell of 1x1x1 under compressive loading conditions. The scaffold unit is created by linear patterning of the unit cell in x, y, and z global coordinates, and is kept larger than the created femur defect. The anatomically matched porous scaffold is constructed using the Boolean intersection of the defected bone with the patterned large scaffold unit. A comprehensive model

with geometry that resembles how a surgeon deburrs the bone prior to implant implantation is created using Boolean operations between big scaffolds and bone that have geometrical overlap. Finally, the scaffold represents the femur model representing the treatment of large defect by anatomically matched scaffold.

### 7.10 Simulation Protocol

The assembled model was imported into ANSYS static structural module for mechanical analysis. The femur geometry meshed with higher-order 3D, 10 node tetrahedral elements (SOLID 187) with an edge length of 2 mm to adequately discretize the strut cross-sections, whereas the scaffold unit was meshed with a tiny edge length of 0.3 mm (Figure 7.18). Table 7.2 shows the number of nodes and elements for each component of the model.


**Figure 7.18:** Illustration of mesh generation a) Femur with solid scaffold a) Femur with anatomically matched P scaffold.

**Table 7.2:** Number of elements and nodes generated in each component of the model for finite element analysis.

| Component | Element Size | Total No. of Elements | Total No. of Nodes |
|---|---|---|---|
| Femur without scaffold | 2 mm | 1,074,830 | 1,612,424 |
| P Scaffold | 0.3 mm | 662,658 | 1,164,054 |
| Solid Scaffold | 2 mm | 2752 | 14,790 |

The material properties of the femur, which were linear orthotropic and assigned uniformly to the femur bone, were adopted from (Reilly et al. 1975) and summarized in Table 7.3. The material model for the scaffold was the same Ti6Al4V alloy that was assigned during the evaluation of the mechanical properties of lattices on compressive loading.

**Table 7.3:** Adopted orthotropic material properties for finite element of femur construct.

| Property | Value |
|---|---|
| Density | $1.8 \times 10^{-6}$ kg-mm$^{-3}$ |
| Engineering Constants | |
| $E_1$ | 11.5 GPa |
| $E_2$ | 11.5 GPa |
| $E_3$ | 17.0 GPa |
| $G_{12}$ | 3.6 GPa |
| $G_{13}$ | 3.28 GPa |
| $G_{23}$ | 3.28 GPa |
| $\nu_{12}$ | 0.58 |
| $\nu_{13}$ | 0.31 |
| $\nu_{23}$ | 0.31 |
| $\nu_{21}$ | 0.58 |
| $\nu_{31}$ | 0.46 |
| $\nu_{32}$ | 0.46 |

Additionally, to identify the difference in stress transfer between porous and solid scaffolds to the surrounding bone, the porous scaffold was replaced with an anatomically comparable solid scaffold and examined under the same physiological loading conditions.

Finally, the model was subjected to loading and boundary conditions for a single leg stance case adopted from the literature (Mann et al. 1994), for which the distal section of the femur was fixed, and hip reaction forces and muscle forces were applied to the model via a selection of the surface of the femur on those locations, as shown in Figure 7.19, and values were tabulated in Table 7.4. A bonded contact was used to avoid sliding between the femur bone scaffold interfaces.

**Table 7.4:** Applied loads on the model.

| **Location** | **Directional Coordinates** | | |
|---|---|---|---|
| | **X** | **Y** | **Z** |
| **Hip Reaction Force (N)** | 1492 | −915 | −2925 |
| **Hip Muscle Force (N)** | −1342 | 832 | 2055 |

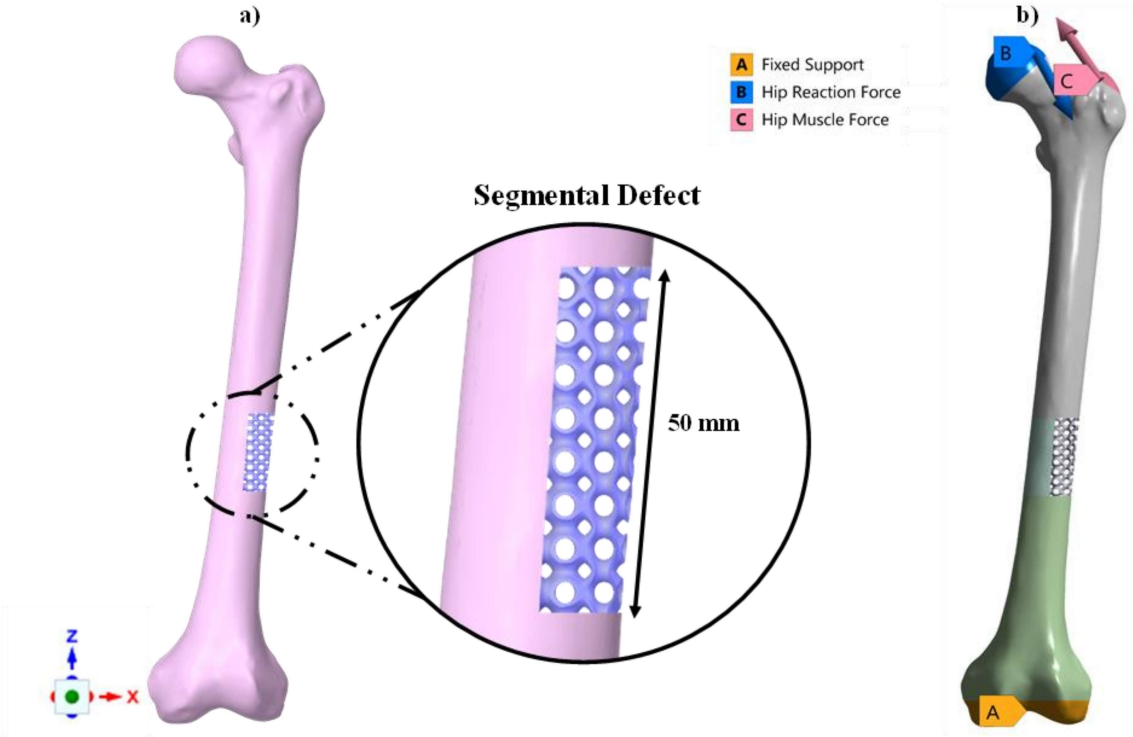


**Figure 7.19:** Typical views of construct (**a**) Femur critical size defect replaced with anatomically matched scaffold (**b**) Loading and boundary conditions on the construct.

### 7.11 Functionality Assessment of Scaffold under Biomechanical Loading

The 3D models of P-based scaffold and solid scaffold mimicking the treatment of critical size bone defects were developed from the method mentioned in above section. The models were analyzed under physiological loading conditions. Von mises stress pattern for the whole femur is illustrated in Figure 7.20. It can be clearly observed that the model with scaffold have shown the higher stress, which is obvious due to the stress concentration at the sharper edges of scaffold.

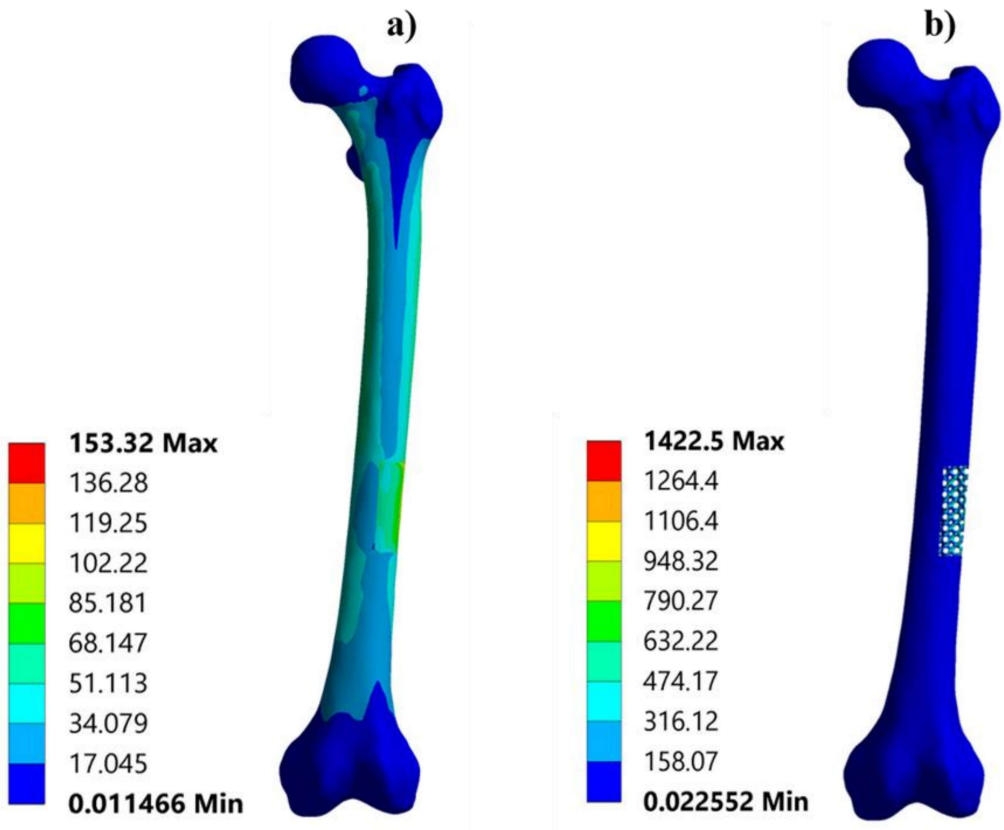


**Figure 7.20:** Von mises stress distribution a) Femur with solid scaffold b) Femur with P scaffold.

Equivalent Von mises stress patterns for solid scaffold and primitive scaffold are shown in Figures 7.21c–f. From Figure 7.21c–e it can be observed that the stress transmission through the bone was 325 MPa when using a porous scaffold. Whereas from Figure 7.21d–f, it can be observed that stress transmission was reduced to 76.204 MPa i.e., a net reduction of approx. 76%, which implied that there was a notable modulus mismatch between the surrounding bone and the solid scaffold. However, using a porous scaffold gives a prominent modulus match between surrounding bone and porous scaffold which leads to more transfer of stresses on the surrounding bone. As a result, when comparing the stress transfer characteristics of porous and solid scaffolds, it is observed that using porous scaffolds provides a promising mechanical stimulus to the bone. The implant interface induces bone tissue regeneration and also subsequent increase in interface strength which promotes restrictions to stress shielding

following bone resorption and implant loosening. Furthermore, to demonstrate the stress concentration on the bone which leads to the stress shielding phenomenon, we adjusted the upper value to 50 MPa of stress on both the models, as shown in Figure 7.21g, h. From the results obtained, as shown in Figure 7.21h, stress concentration was observed in the top left area (red-colored region) which signified that the stress shielding effect was very high when using a solid scaffold. On the contrary, from Figure 7.21g, it could be observed that when a porous scaffold was used, stress concentration was not at particular locations, instead it was equally distributed to the area of bone and scaffold interface. However, due to manufacturing errors that substantially cause a reduction in mechanical properties, the FEA of scaffolds approximates the mechanical properties of additively produced scaffolds. According to previous studies, surface roughness can cause a 66 percent increase in finite element analysis findings (Cahill et al. 2009). As a result, it is always essential to obtain the relation between constructed scaffold parameters and overall mechanical properties for each scaffold, as well as additive manufacturing features, for the purpose of confirmed validation and referencing for scaffold functionality, especially in patient-specific scenarios.

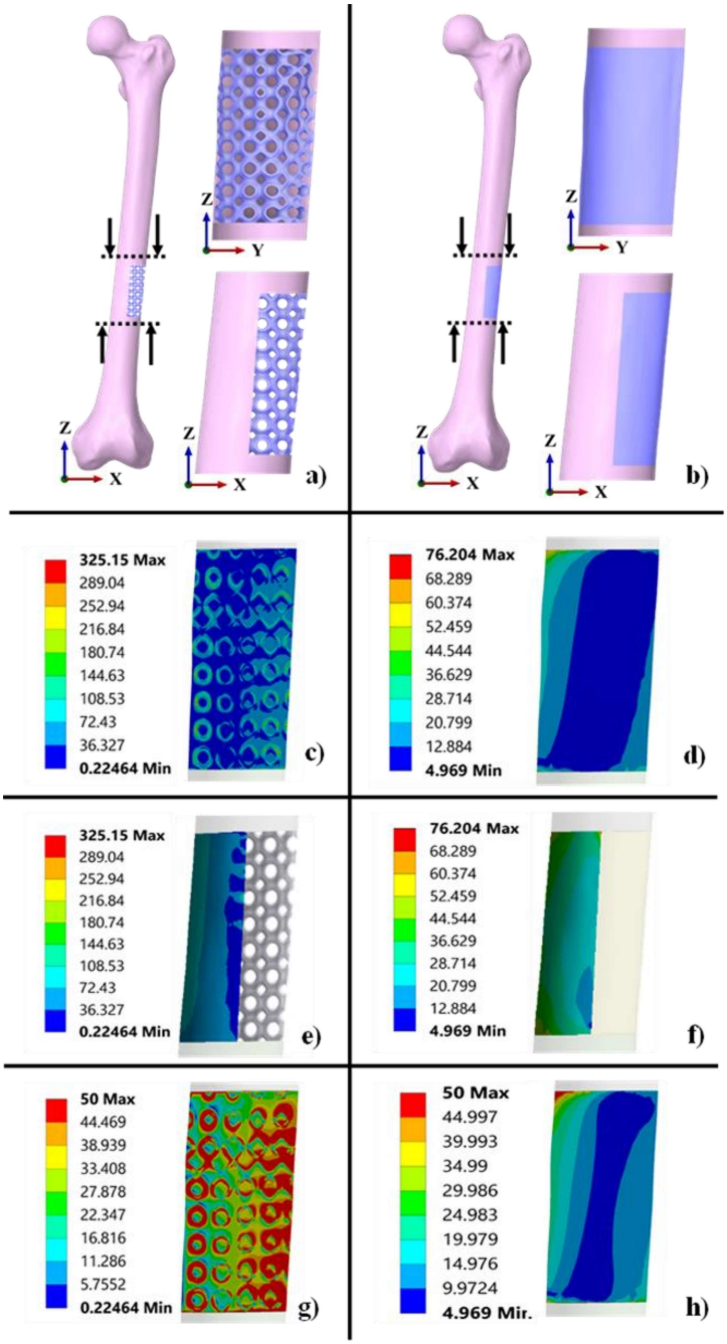


**Figure 7.21:** Biomechanical setup of the critical size bone defect with solid and porous scaffolds on femur bone to demonstrate the stress transfer patterns (a). The femur bone defect replaced with P lattice structures with 80% porosity (top right shows the enlarged lateral view and bottom right shows the front view illustrating the defect where bone fragments have contact. (b) The femur bone defect replaced with solid scaffold. (c) Stress transmission pattern on the bone at P scaffold and bone interfaces after removing scaffold. (d) Stress transmission pattern on the bone at solid scaffold and bone interfaces after removing solid scaffold. (e) Von Mises stress patterns of bone with porous scaffold (Front view). (f) Von Mises stress patterns of bone with porous scaffold (Front view). A threshold of the maximum value of 50 MPa was set to visualize the stress concentration in the (g) Model with P scaffold and (h) Model with a solid scaffold.

## 7.12 Summary

The structural design and analysis of the TPMS-based porous scaffold is an important factor for determining the pre-clinical performance of the implant to treat segmental bone defects. The morphological properties (pore shape and size, strut thickness, and porosity) of porous scaffolds are the basic controlling parameters that greatly influence their overall performance. However, an optimum balance between the structural-mechanical properties to obtain complex porous structures and their integrity at specific locations is challenging.

In comparison to the solid scaffolds, the porous P-based TPMS structures effectively reduced the stress shielding phenomenon which suggests that TPMS-based porous structures have the potential to reduce the stiffness mismatch between the bone-implant interface. A further extensive study will illustrate the full potential of the suggested TPMS-based (P and G) scaffolds on the grounds of experimental investigation to study the strength and failure mechanisms at various modes of loading, computational and experimental investigations for permeability analysis, and clinical validation for assessing real scenarios of biocompatibility and tissue responses.